Maximizing Wave Energy Converter Power Extraction by Utilizing a Variable Negative Stiffness Magnetic Spring

Jeff T. Grasberger, Ryan G. Coe, Giorgio Bacelli, Jonathan Bird, Alex Hagmüller, and Carlos A. Michelén Ströfer

***Abstract*—Complex conjugate impedance matching is a key concept for wave energy converter design. Matching the impedance of the power take-off (PTO) system to the complex conjugate of the wave energy converter's (WEC) impedance ensures efficient transfer of energy from the WEC body motion to electrical power. In low frequency waves, impedance matching often requires a negative PTO stiffness. In this paper, an adjustable stiffness magnetic torsion spring will be presented and modeled to understand its potential to improve WEC performance. The spring has the ability to provide a negative stiffness, allowing the PTO impedance to more closely match the complex conjugate of the WEC impedance at low frequencies. The spring also supports an adjustable stiffness value, meaning it can be tuned according to the incoming wave conditions. The spring's tunability may put less stress on the rest of the PTO system in wave conditions outside its normal operation zone without sacrificing electrical power output. The adjustable magnetic spring's effects are modeled and explored in this paper by examining the resultant average annual electrical power and capacity factor. The study suggests that the tunable magnetic spring has the potential to significantly improve capacity factor while maintaining a high average electrical power.**

***Index Terms*—Wave energy converter (WEC), power take-off (PTO), optimization, co-design, optimal control**

I. Introduction

To maximize wave energy converter (WEC) power extraction, the power take-off (PTO) of the WEC generator should be tuned to match the complex conjugate of the WEC [1]. For longer period, low frequency, wave conditions which contain much of the world's ocean wave energy [2], matching the PTO impedance to the complex conjugate of the WEC device requires either increasing the mass of the WEC or decreasing the stiffness of the PTO. A negative PTO spring stiffness, for instance, can effectively make the PTO impedance closer to the complex conjugate of the WEC device's intrinsic impedance in low frequency oscillation. If the PTO spring stiffness can be controlled to have a negative value, the WEC can be made relatively small, and low cost, but still achieve impedance matching. Furthermore, a PTO spring stiffness which can be tuned can ensure efficient energy transfer across a wide array of sea states.

One approach to making the PTO operate with a negative stiffness spring constant involves designing a generator to provide a force that mimics a negative spring constant. Such an approach was studied in [3]. The generator voltage and current are related to the WEC damping and stiffness terms respectively. Therefore, to provide both a sizable generator damping as well as negative stiffness the generator voltage and current must be highly out of phase and thus an extremely large amount of reactive power must be created by the generator. This demand vastly increases the generator and power electronic converter cost [3]. Another option to support WEC-PTO impedance matching is to use a mechanical or pneumatic spring with a negative spring constant [4]. However, the long-term reliability of such a PTO within the harsh ocean environment may be questionable. In addition, the efficiency of pneumatic springs is limited.

This paper will present a WEC and PTO simulation and analysis when utilizing a newly developed adjustable stiffness (AS) magnetic torsion spring (MTS) [5]. The negative stiffness value can be adjusted through the relative motion of the rotors. The AS-MTS can not only provide a negative spring stiffness, but is also adjustable and can thus be tuned according to the current wave conditions. The negative spring stiffness of the AS-MTS can alter the overall PTO impedance to match the complex conjugate of the WEC without sacrificing significant reliability, efficiency, or large reactive power. Furthermore, the tunability of the AS-MTS may put less stress on the rest of the PTO in wave conditions outside of normal operation while still supporting increased power capture when compared to a constant stiffness spring.

The performance benefits of the AS-MTS within a point absorber WEC will be detailed and the results of the simulation analysis when using WecOptTool[1] will be presented. WecOptTool is an open-source WEC optimization software that supports efficient PTO and control optimization. WecOptTool will be used to assess the WEC PTO system performance with the adjustable stiffness magnetic torsion spring relative to the

This research was supported by the U.S. Department of Energy's Water Power Technologies Office.

J. T. Grasberger, R. G. Coe, G. Bacelli, and C. A. Michelén Ströfer are with Sandia National Laboratories, Albuquerque, NM 87123, U.S.A. (e-mail: [jtgrasb, rcoe, gbacell, cmichel]@sandia.gov)

J. Bird is with Portland State University, Portland, OR 97201, U.S.A. (e-mail: bird@pdx.edu)

A. Hagmüller is with AquaHarmonics Inc., West Linn, OR 97068, U.S.A. (e-mail: alex.hagmuller@aquaharmonics.com)

[1]WecOptTool: https://github.com/sandialabs/WecOptTool

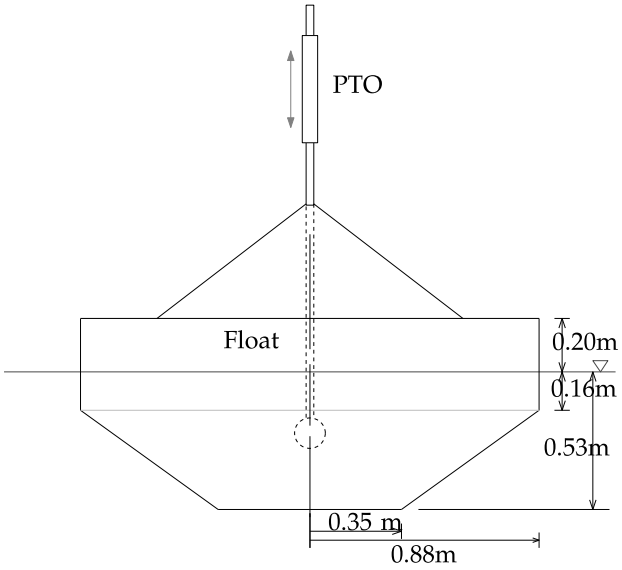

Fig. 1. WaveBot device [6] with dimensions.

design goal of achieving a high capacity factor while maintaining significant annual average electrical power in a set of scaled-down realistic sea states.

II. System Dynamics

A. WEC Dynamics

A point absorber WEC known as the WaveBot is used to complete this study (Fig. 1). Point absorbers can be linearly modeled based on the time-domain residual form (r(t) = 0) in (1).

$$r(t) = M\ddot{z} - f_r(t) - f_h(t) - f_f(t) - f_e(t) - f_a(t) \quad (1)$$

Here, M is a mass/inertia matrix, $\ddot{z}$ the WEC acceleration vector, and the different generalized force vectors are the radiation force f_r due to wave generation, the hydrostatic force f_h, the hydrodynamic frictional force f_f, the wave excitation force f_e, and any additional forces f_a such as PTO and mooring forces. The hydrodynamic forces listed above are obtained from solutions to the radiation and diffraction problems using the boundary element method code `Capytaine`[2] [7].

The wave energy converter dynamics can also be understood through the calculation of the device's intrinsic impedance. The impedance is a ratio of the device response velocity to the input force from the waves, defined by (2). The input forces from the wave can be easily related to the WEC response with the impedance, making it valuable to WEC design.

$$Z_i(\omega) = j\omega(M + A(\omega)) + B(\omega) + B_f + \frac{K_{hs}}{j\omega} \quad (2)$$

With an understanding of the WEC intrinsic impedance, the theoretical maximum mechanical power absorbed by the WEC [8] can be derived in (3).

[2]*Capytaine:* https://ancell.in/capytaine/latest/

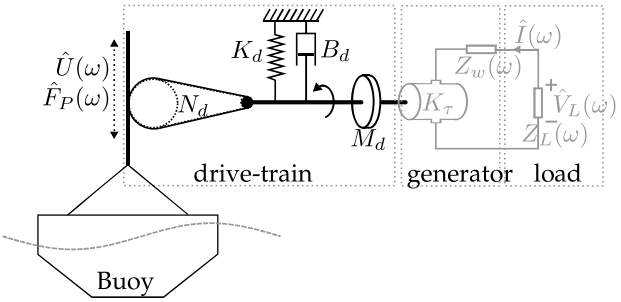

Fig. 2. Wave-to-wire model of the WaveBot illustrating the energy conversion chain and the main parameters driving the dynamics. The drive-train parameters are printed in black font and drive the mechanical power conversion. The generator and load parameters are printed in grey font and drive the electromagnetic and electrical energy conversion, respectively, with Z_L as the load impedance.

The maximum mechanical power is not generally realistically achievable, but will serve as a comparison tool in this study.

$$P_{max} = \frac{|f_e|^2}{8\Re\{Z_i\}} \quad (3)$$

B. PTO Dynamics and Electrical Power

The power take-off for the WaveBot is detailed in Fig. 2. It includes a belt transmission mechanism that converts the heave motion to rotational shaft motion. This is modeled with an effective gear ratio with units of rad/m. As built, the rotational shaft is connected directly to the generator, but here we consider the addition of the adjustable stiffness magnetic torsion spring to beneficially alter the dynamics of the system, which also has an associated gear ratio. Following the spring, the shaft is connected to a three-phase permanent magnet synchronous generator, which is modeled with the linear power-invariant Park transform [9]. The transform can be applied to any AC electric machine and results in a linear time-invariant system. Since the resulting model is linear, it can be represented in terms of an impedance matrix. Although, this is a simplified linear model, it captures the most relevant dynamics for electromagnetic energy conversion including I^2R losses. Therefore, the model presented in this section is applicable to a wide range of WEC PTOs.

The PTO can be modeled as a two-port network for simplicity [10]. Thus, an impedance matrix for the power take-off is expressed as

$$\begin{bmatrix} \hat{F}_p(\omega) \\ \hat{V}(\omega) \end{bmatrix} = \begin{bmatrix} Z_{11} & Z_{12} \\ Z_{21} & Z_{22} \end{bmatrix} \begin{bmatrix} \hat{U}(\omega) \\ \hat{I}(\omega) \end{bmatrix}, \quad (4)$$

where the flow variables: velocity $\hat{U}(\omega)$ and load current $\hat{I}(\omega)$, are related to the effort variables: PTO force $\hat{F}_p(\omega)$ and load voltage $\hat{V}(\omega)$, by a PTO matrix with

$$Z_{11} = -N_d^2 Z_d(\omega) \quad (5a)$$

$$Z_{12} = -\sqrt{\frac{3}{2}} K_\tau N_d \quad (5b)$$

$$Z_{21} = -\sqrt{\frac{3}{2}} K_\tau N_d \quad (5c)$$

TABLE I
WAVEBOT DEVICE NOMINAL DESIGN PARAMETERS.

Parameter	Value
Rigid body mass, M [kg]	874
Hydrostatic stiffness, K_{hs} [N/m]	24.4E3
Gear ratio, N_d [rad/m]	12.4666
Spring gear ratio, N_s [ ]	0.25
Torque constant, K_τ [N m/A]	6.1745
Winding resistance, B_w [Ω]	0.5
Winding inductance, L_w [H]	0
Drive-train inertia, M_d [kg m^2]	2
Drive-train linear friction, B_d [N m s/rad]	1
Drive-train stiffness, K_d [N m/rad]	0

$$Z_{22} = Z_w(\omega) \tag{5d}$$

Here, N_d is the gear ratio and K_τ is the torque constant that relates electrical current to electromagnetic torque. The drive-train impedance Z_d and generator winding impedance Z_w can be described in terms of drive-train inertia M_d, resistance B_d, stiffness K_d, and spring gear ratio N_s, and winding inductance L_w and resistance B_w, respectively, in (6) and (7).

$$Z_d(\omega) = -j\omega M_d + B_d + j\frac{1}{\omega}K_d\,N_s^2 \tag{6}$$

$$Z_w(\omega) = -j\omega L_w + B_w \tag{7}$$

The nominal (as-built) component parameters for the WaveBot PTO system are shown in TABLE I. Each of these values are kept constant throughout this study except for the drive-train stiffness which represents the adjustable stiffness magnetic torsion spring.

To design an efficient WEC and PTO system, the power conversion both from the WEC to the PTO and the PTO to the load should be considered. Maximum power transfer occurs when complex conjugate impedance matching is achieved on both the input side (between intrinsic WEC impedance and PTO input impedance) and on the output side (between PTO output impedance and load impedance). The PTO is a complex system, but the two-port network representation allows for derivation of the input and output impedance. The PTO input impedance in (8) is the impedance experienced at the input of the two-port network.

$$Z_{in} = -Z_{11} + \frac{Z_{12}Z_{21}}{Z_{22} + Z_L} \tag{8}$$

Here, Z_L is the load impedance and is optimal when equal to the complex conjugate of the PTO output impedance in (9).

$$Z_L = [Z_{22} + \frac{Z_{12}Z_{21}}{-Z_{11} + Z_i}]^* \tag{9}$$

Assuming the load impedance can be controlled to match the PTO output impedance, the PTO input impedance can be altered by adjusting the components of the PTO to match the complex conjugate of the WEC intrinsic impedance in the desired wave conditions. This study focuses on using the AS-MTS to tune the drive-train stiffness value, which supports impedance matching between the WEC and PTO according to input wave conditions.

C. Optimization Problem

The optimization process used for this study is considered a pseudo-spectral method [11]–[13]. A Fourier decomposition of the WEC position is completed for a discrete frequency array $\omega = [\omega_0, 2\omega_0, \ldots, N_\omega\omega_0]$ of length N_ω, where ω_0 is the fundamental frequency. An unstructured optimal controller, which can apply an arbitrary PTO force at each time step, is used in this study. Thus, the control coefficients are formatted as an array of equal length to the WEC position array. The Fourier and control coefficients are stored together in a single state variable (x). When also optimizing the AS-MTS, the drive-train stiffness value K_d is appended to the end of the state variable to be included in the optimization. The optimization problem in (10) can then include solving for the WEC dynamics, the optimal control state, and the drive-train stiffness to minimize the objective function.

$$\begin{aligned} \min_x \quad & J(x) \\ \text{s.t.} \quad & \\ & r(x) = 0 \\ & c_{ineq}(x) \geq 0 \\ & c_{eq}(x) = 0, \end{aligned} \tag{10}$$

Here, $J(x)$ is the objective function (e.g., average electrical power), $r(x)$ captures the WEC dynamics in residual form (Section II-A), and c_{eq} and c_{ineq} are arbitrary equality and inequality constraints. In this study, the objective function is the average electric power, and an inequality constraint is applied for some specified cases to limit the maximum RMS power.

III. DESIGN FOR A SINGLE SEA STATE

The adjustable stiffness magnetic torsion spring is assumed to take on any stiffness value necessary to optimize the objective function. For small heaving WECs and relatively low frequency (long period) waves, which make up most of the world's harvestable wave energy, a negative spring stiffness is very often optimal. A negative drive-train spring stiffness changes the PTO impedance, making it closer to the complex conjugate of the WaveBot intrinsic impedance. Fig. 3 shows an example where the real and imaginary part of the complex conjugate of the intrinsic impedance (Z_i^*) and the PTO input impedance (Z_{PTO}) are plotted for increasingly negative drive-train stiffness (K_d) values. The negative stiffness shifts the PTO impedance toward the complex conjugate of the intrinsic impedance at the wave frequency (0.3 Hz) which induces maximum power transfer from the waves to the PTO.

By shifting the PTO input impedance toward the complex conjugate of the intrinsic impedance, the transfer of power from the WaveBot device to the PTO system is improved significantly. This difference can be seen using an energy flow diagram to compare a design with zero spring stiffness to one with an

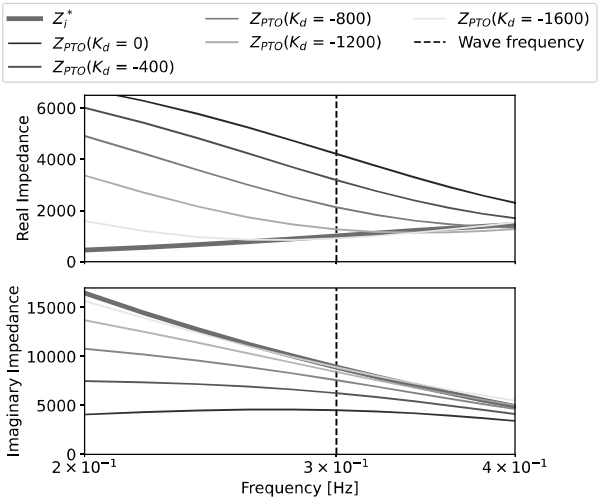

Fig. 3. For increasingly negative spring stiffness (Nm/rad) up to the optimal (-1614 Nm/rad), the real and imaginary parts of PTO impedance (Z_{PTO}) shift toward to the complex conjugate of the WaveBot's intrinsic impedance (Z_i^*).

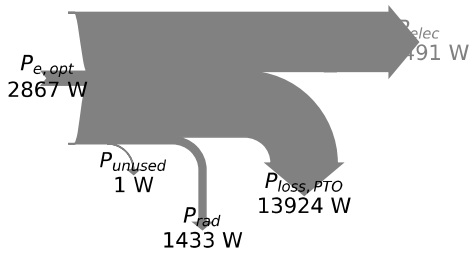

Fig. 4. Power flow diagram for WaveBot design with zero drive-train stiffness in regular wave conditions with $T_e = 3.33$ s and $H_{m0} = 0.2$ m and controls optimized for maximum mechanical power. Mechanical power optimization leads to the maximum energy absorbed by the WaveBot, but also requires an extremely large amount of input electrical power.

optimized spring stiffness in a regular wave with a frequency of 0.3 Hz and an amplitude of 0.2 m. The energy flow diagram details the input energy and output energy of the system, with the flows calculated by

$$P_{e,opt} = 2P_{max} \tag{11a}$$

$$P_e = \frac{1}{4}(f_e U^* + f_e^* U) \tag{11b}$$

$$P_{unused} = P_{e,opt} - P_e \tag{11c}$$

$$P_{rad} = \frac{1}{2}\Re\{Z_i\}|U|^2 \tag{11d}$$

$$P_{mech} = f_P U \tag{11e}$$

$$P_{elec} = i_L v_L \tag{11f}$$

$$P_{loss,PTO} = P_{mech} - P_{elec}, \tag{11g}$$

where $P_{e,opt}$ is the optimal excitation power, P_e is the actual excited power of the WEC, P_{unused} is the unused power not absorbed or radiated by the WEC, P_{rad} is the power radiated by the WEC, P_{mech} is the mechanical power based on WEC velocity U and PTO force f_P, P_{elec} is the electrical power harvested by the load, and $P_{loss,PTO}$ comprises the losses within the PTO and electrical power conversion.

First, a dramatic example of the power flow diagram for the WaveBot with the unstructured controller optimized for maximization of mechanical power is shown in Fig. 4. The mechanical power maximization leads to the maximum potential mechanical power according to (3). The mechanical power maximization is achieved at the expense of extremely large electrical power that needs to be *input* into the system. Although the electrical power arrow is shown as an output, the red font and negative sign are used to indicate the required electrical power input. The optimal excitation power $P_{e,opt}$ from the waves is almost completed absorbed by the WEC as indicated by $P_{unused} = 1W$, but any absorbed power is dwarfed by the electrical power input and subsequently lost in the PTO power conversion. Not only is the system's electrical power far from optimal (in fact, it consumes electrical power rather than generating it), but even if operated in a way that does produce net electrical power would require a PTO with an extremely large and expensive power rating.

Returning to more practical scenarios, with zero stiffness (Fig. 5a) and optimized for electrical power maximization, the system is able to support a small amount of electrical power harvest. However, the electrical power realization allows for more accurate (and less expensive) PTO design according to a realistic power rating. Still, relatively large levels of power are left unused, meaning it is not absorbed or radiated by the WEC. It is important to note that maximum power transfer from waves to WEC requires 50% of the absorbed power to be radiated out by the WEC. The large amount of unused power as well as power take-off losses prevent the system from converting the maximum absorbable power as calculated by (3) to electrical power.

On the other hand, with an optimally tuned spring (Fig. 5b) and electrical power optimization, the PTO impedance closely matches the complex conjugate of the intrinsic impedance at the wave frequency as shown previously in Fig. 3. Significantly less power is left unused, meaning more power is absorbed by the WEC and much closer to 50% of the optimal excited power is radiated out by the WEC. The PTO losses are relatively similar for both the zero and tuned results despite the tuned stiffness leading to about three times larger velocity. Since friction is proportional to the square of velocity, over ten times as much power (187 vs. 18 W) lost in the PTO is due to friction for the negative versus zero stiffness result. Despite much larger friction losses, similar PTO losses mean that the complex conjugate impedance matching between the WEC and PTO as a result of the optimized negative drive-train stiffness leads to much lower relative PTO

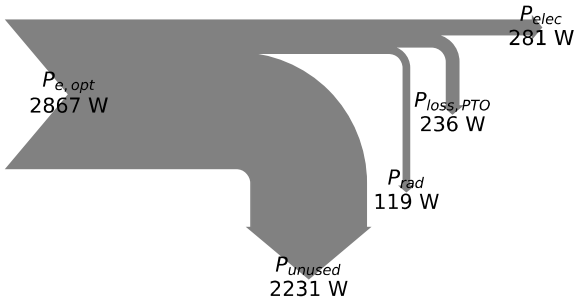

(a) Zero drive-train stiffness

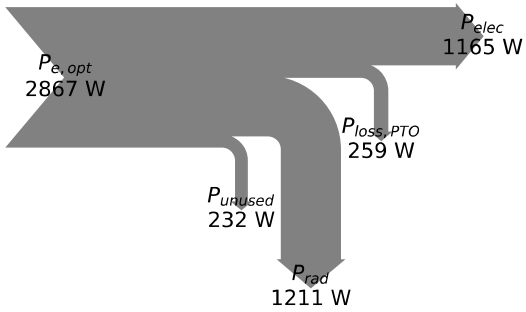

(b) Optimally tuned drive-train stiffness

Fig. 5. Power flow diagrams for WaveBot in regular wave conditions with $T_e = 3.33\,\mathrm{s}$ and $H_{m0} = 0.2\,\mathrm{m}$. With zero stiffness, the system fails to absorb large amounts of power from the waves and converts only a small amount of the available excitation power to electrical power. With a tuned negative stiffness, the system absorbs much greater power from the waves and also contributes to larger radiated power. Despite significant friction losses due to the larger WEC energy, PTO losses are relatively low and electrical power is significantly improved when compared to the zero stiffness case.

power losses.

IV. Design for Average Annual Performance

A. Sea States

To understand the potential of the AS-MTS, the system needs to be tested in realistic sea states. Fig. 6 shows hourly sea states loaded from the PacWave site which were scaled down (12:1) to more closely match the scale of the WaveBot design. Each white X mark indicates the center of a cluster of similar waves derived using k-means clustering. The cluster centers are each used to create a JONSWAP spectrum with a peak enhancement factor $\gamma = 3.3$ as shown in Fig. 7. One potential benefit of the tunable spring design is the ability to alter the spring stiffness according to each sea state. By testing the design across 10 sea states, the relative benefit of the spring tunability can be understood.

For a given design, the average annual power is obtained as a weighted average (according to occurrence of cluster conditions) of the average electrical power $P_{elec} = v(t)i(t)$ for each sea state.

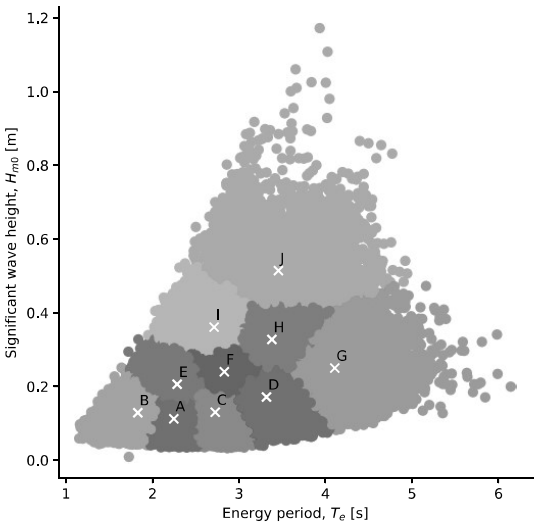

Fig. 6. PacWave location sea states (scaled down 12:1) discretized into 10 clusters using k-means. All 1-hour sea states are shown for the 25 year period from 1997-2021. The center of each cluster is indicated with an 'x' mark.

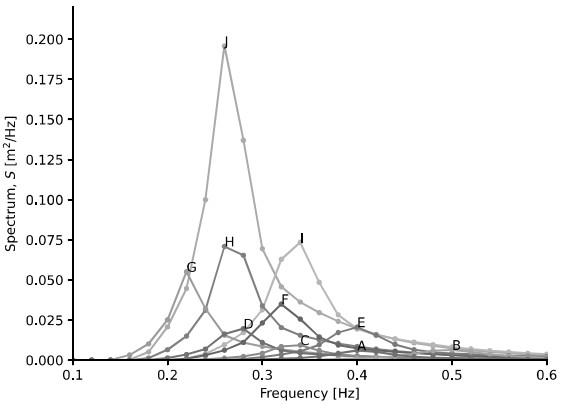

Fig. 7. JONSWAP spectrum for each of the ten representative sea states used in the annual power estimate.

B. Baseline Comparison in 10 Sea States

For each of the 10 sea state clusters identified in Section IV-A, the AS-MTS can be tuned to implement a different spring stiffness value. The potential benefits of the AS-MTS can be understood in terms of electrical power output by including the linear PTO and unstructured controller. Fig. 8 shows the electrical power results for 3 different setups without considering any constraints. First, the solid green line shows the theoretical maximum mechanical power in each sea state according to (3). The dashed green line shows the results for the tunable spring stiffness (based on AS-MTS design). To compare to an optimal constant spring stiffness value, the optimal spring stiffness for the total average sea state was found and applied to all 10 sea states. These results are indicated by the orange

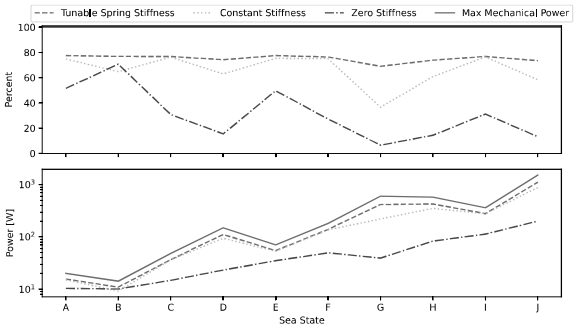

Fig. 8. Electrical power in 10 sea state clusters with AS-MTS as compared to constant spring coefficient and zero spring stiffness. Top axes (percent) corresponds to the percent of the theoretical maximum mechanical converted to electrical power.

line which has a constant negative spring stiffness. Lastly, the blue line illustrates the results of a system with zero spring stiffness without an AS-MTS. It is clear from the bottom axes in Fig. 8 that the tunable spring design allows for much larger electrical power harvest in all sea states than the zero stiffness design and a slightly larger harvest than the constant stiffness design in some sea states. The top set of axes indicates the percentage of the maximum theoretical power achieved in each sea state by the three spring designs. This more clearly illustrates the difference between the tunable and constant stiffness designs. A tunable stiffness value allows the system to more consistently achieve about 80% of the maximum theoretical power, while the constant stiffness design experiences much more variance and achieves less than 50% in some sea states with longer or shorter wave periods than what its designed for.

The annual average and maximum parameter values for the 3 different spring stiffness designs are shown in TABLE II. As stated previously, the tunable spring is able to extract the greatest average annual electrical power. In order to better understand the associated costs with each design, the required rated power for a corresponding generator should be found. The required rated power corresponds to the highest root mean square (RMS) power throughout all of the sea states. The RMS power value is greatest for the tunable spring design and smallest with zero stiffness. The capacity factor is defined here as the ratio of annual average power to the rated (RMS) power and provides an idea of the ratio of potential revenue to cost. The tunable spring design has a better average capacity factor than the constant stiffness but less than the zero stiffness design. A better capacity factor in itself does not mean that the zero stiffness design is better than the tunable spring, but it does suggest the current unconstrained result may not be optimal from a capacity factor standpoint due to the large rated power.

For comparison, wind turbines and photovoltaic arrays often have much larger capacity factors between 30% and 35% [14]. The capacity factors noted in TABLE II are much lower because the optimization problem is set up to maximize power at all costs. The

TABLE II
ANNUAL RESULTS FOR 3 SPRING STIFFNESS DESIGNS ("TUNABLE:" NEGATIVE SPRING STIFFNESS TUNED TO SUIT EACH SEA STATE, "CONSTANT:" NEGATIVE SPRING STIFFNESS FIXED FOR ALL SEA STATE, "ZERO:" NO NEGATIVE SPRING PRESENT).

Variable (annual)	Tunable	Constant	Zero
Mean Electrical Power [W]	132.3	113.3	37.9
Mean % of Maximum Power [ ]	76.3	70.3	39.8
Maximum RMS Power [W]	1870	1820	440
Mean Capacity Factor [ ]	0.071	0.062	0.086
Peak Power [W]	6630	6610	1770
Maximum PTO Force [N]	3650	5200	4020
Maximum Position [m]	1.70	1.23	0.34

objective of the unstructured controller is to maximize electrical power, which also increases the RMS power, meaning the current solution does not address capacity factor at all. This sub-optimality in terms of capacity factor will be investigated further through the addition of a constraint on the RMS power in Section IV-C.

The ability of the tunable spring to more consistently absorb and convert mechanical to electrical power is clearly beneficial, but still leads to greater RMS power, peak power, and heave motion than for the constant and zero stiffness designs. It is worth noting that these factors would require more expensive PTO design. On the other hand, the lower required PTO force for the tunable stiffness would mean the required torque rating could potentially be reduced (lowering cost). Each of these factors contribute to the cost of the PTO system, but are likely a facet of the previously mentioned sub-optimal problem setup which maximizes power at all costs.

C. Improving Capacity Factor

In Section IV-B, the WaveBot is tested in 10 different representative sea states to compare the AS-MTS to constant and zero spring stiffness designs without any constraints considered. Ultimately, the goal of this study is to focus on designing a system that can achieve a high ratio of potential revenue to cost. Here, the capacity factor is defined as the ratio of the average annual power to the RMS power, which can be used as an approximate ratio of revenue to cost. The tunable spring has the potential to increase average annual power, but the RMS power requires consideration of controls. The unstructured controller can quickly and effectively apply a constraint on the RMS power. By constraining the RMS power while optimizing for maximum electrical power, it is expected that the total capacity factor can be increased.

Fig. 9 shows the results of the application of an RMS constraint of various values from 50 W to 1500 W in 50 W increments. As a tighter RMS constraint is applied, the average annual power decreases, but at a slower rate than the applied RMS constraint. Thus, the ratio of average power to RMS power, also known as the capacity factor, increases with decreasing RMS constraint value. In summary, tightening the RMS constraint decreases the average power but increases the capacity factor. The top two axes in Fig. 9 are

valuable because they clearly details two opposing design objectives. Increasing the capacity factor leads to an economically advantageous design but at the cost of the total electrical power harvested by the system. The optimal RMS constraint value requires an understanding of the revenue based on the average power and the exact cost associated with the rated power. Somewhere within this range of applied RMS constraint values exists an optimal solution where a high capacity factor is achieved without significant sacrifices in the annual average power.

When comparing the 3 different spring designs, it is clear that the tunable spring performs better than the constant and zero stiffness designs across all RMS constraint values tested in terms of both the average annual power and the capacity factor. As shown in Section IV-B, the zero stiffness system has a relatively small average power even when unconstrained, and thus is only affected when a relatively tight (< 400 W) RMS constraint is applied. Although the unconstrained example shows a higher capacity factor associated with zero stiffness, it is clear that the RMS constraint has a greater positive effect on the tunable and constant stiffness designs, increasing the capacity factor across all constraint values tested. Throughout the entire range of constraints, the constant stiffness results in relatively similar, albeit slightly smaller, average annual power and capacity factor when compared to the tunable stiffness.

To properly evaluate the tunable spring stiffness design as well as the implementation of the RMS constraint, the resultant dynamics in terms of the WEC and PTO response need to be better understood. Parameters such as the maximum heave position, peak power, and maximum PTO force also contribute to the cost and impact the design of the overall system. The third and fourth axes in Fig. 9 show the maximum heave position and the peak power for the different systems considered. The tunable spring system experiences the largest maximum position, which seems to be slightly limited by the RMS constraint. The peak power increases relatively similarly for each of the 3 designs up until the RMS constraint exceeds about 600 W where the zero stiffness system experiences a consistently smaller peak power. The last three axes in Fig. 9 the maximum PTO force, spring torque, and spring rotation. The maximum PTO force does not seem to be significantly affected by the RMS constraint. Regardless of RMS constraint, the tunable stiffness system leads to a smaller maximum PTO force than the zero and constant stiffness systems. Lastly, the maximum spring force and rotation are both linked directly to the maximum heave position so their trends are exactly the same (except for the zero spring stiffness case).

In order to select an optimal RMS constraint value, each of the above factors must be considered along with their resulting costs. One potential solution pairs the tunable spring design with an RMS constraint of 250 W, which leads to an average annual power of 81 W and a capacity factor of 0.325. This solution is able to harvest almost two-thirds of the power when compared to the unconstrained case in TABLE II while requiring a relatively low RMS and peak power. Thus,

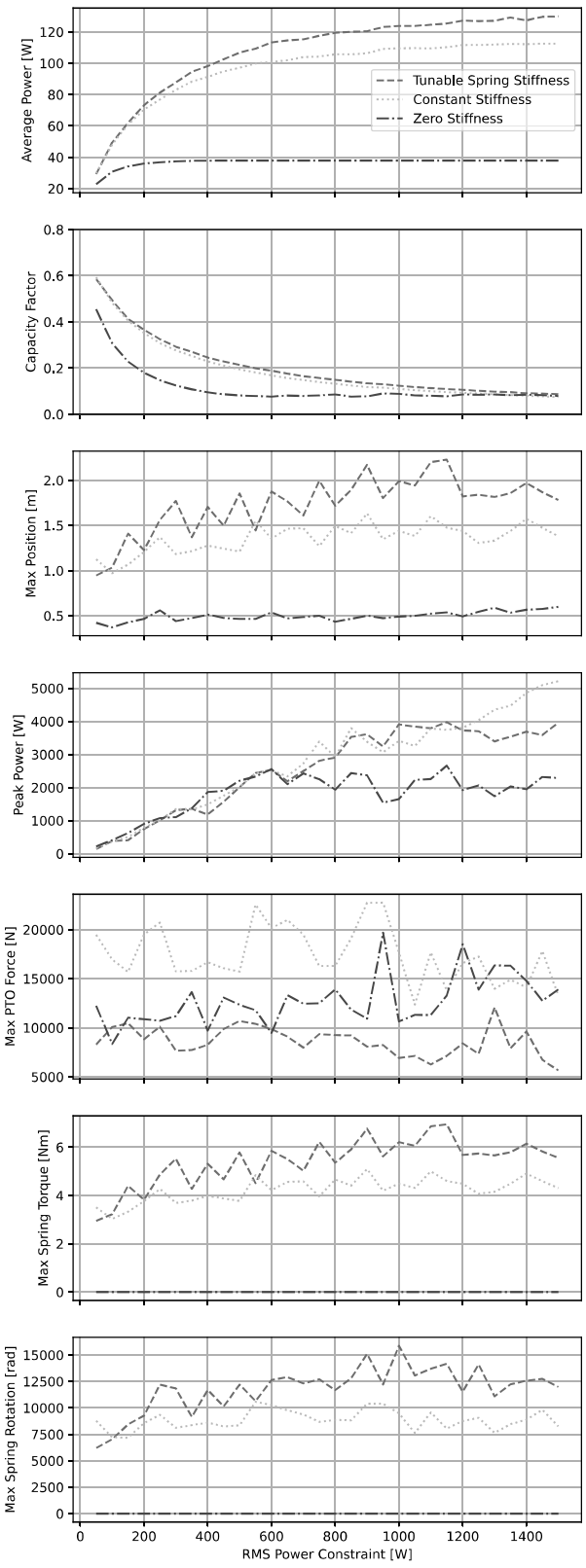

Fig. 9. Average annual power, capacity factor, maximum heave position, peak power, maximum PTO force, spring torque, and spring rotation with varying RMS constraint values for tunable, constant, and zero stiffness systems.

the capacity factor is almost five times as large and annual average power only reduced by less than half. Although the tunable spring design does not significantly outperform the constant negative spring stiffness design in terms of electrical power and capacity factor, it requires about half the PTO force.

Because the exact cost of the components is yet to be determined, the potential solution cannot be fully evaluated. The potential solution can still be evaluated through various comparisons. In [15], the capacity factor of multiple WECs are analyzed and are mostly between 10% and 25% despite significant variation between types and locations. The potential solution identified here using the AS-MTS design and constraining the RMS power would provide a significant improvement in capacity factor over most other WEC designs. Wind energy, being far ahead of wave energy in terms of commercialization, also provides a valuable comparison. Wind turbines experience similarly large ranges of conditions which lead to capacity factors in the range of 30% to 35% [14]. Thus, the potential solution here could be competitive with the wind industry in terms of capacity factor.

V. Conclusion

A negative drive-train stiffness supports complex conjugate impedance matching between the WaveBot WEC and its power take-off system which can lead to optimal power transfer from WEC to PTO. By including an adjustable stiffness magnetic torsion spring as part of the PTO system, the drive-train stiffness can be tuned according to the sea state to maximize electrical power. When compared to zero and constant stiffness designs, the AS-MTS model leads to greater average annual electrical power for a set of realistic, scaled-down sea states. The introduction of a constraint on the rated (RMS) power allows for an increase in the capacity factor at the expense of average annual power. The implementation of the rated power constraint with the tunable spring stiffness supports a complex multi-objective evaluation which considers two competing goals of maximizing both capacity factor and electrical power.

Acknowledgement

This research was supported by the U.S. Department of Energy's Water Power Technologies Office. Sandia National Laboratories is a multi-mission laboratory managed and operated by National Technology and Engineering Solutions of Sandia, LLC., a wholly owned subsidiary of Honeywell International, Inc., for the U.S. Department of Energy's National Nuclear Security Administration under contract DE-NA0003525. This paper describes objective technical results and analysis. Any subjective views or opinions that might be expressed in the paper do not necessarily represent the views of the U.S. Department of Energy or the United States Government.

References

[1] R. G. Coe, G. Bacelli, D. G. Wilson, O. Abdelkhalik, U. A. Korde, and R. D. Robinett III, "A comparison of control strategies for wave energy converters," *International journal of marine energy*, vol. 20, pp. 45–63, 2017. [Online]. Available: https://doi.org/10.1016/j.ijome.2017.11.001

[2] P. Lenee-Bluhm, R. Paasch, and H. T. Özkan-Haller, "Characterizing the wave energy resource of the US Pacific Northwest," *Renewable Energy*, vol. 36, no. 8, pp. 2106–2119, 2011. [Online]. Available: https://doi.org/10.1016/j.renene.2011.01.016

[3] J. K. Shek, D. E. Macpherson, M. A. Mueller, and J. Xiang, "Reaction force control of a linear electrical generator for direct drive wave energy conversion," *IET renewable power generation*, vol. 1, no. 1, pp. 17–24, 2007. [Online]. Available: https://digital-library.theiet.org/content/journals/10.1049/iet-rpg_20060028

[4] J. H. Todalshaug, G. S. Ásgeirsson, E. Hjálmarsson, J. Maillet, P. Möller, P. Pires, M. Guérinel, and M. Lopes, "Tank testing of an inherently phase-controlled wave energy converter," *International Journal of Marine Energy*, vol. 15, pp. 68–84, 2016. [Online]. Available: https://doi.org/10.1016/j.ijome.2016.04.007

[5] D. Che, B. Dechant, A. Hagmüller, and J. Z. Bird, "A multi-stack variable stiffness magnetic torsion spring for a wave energy converter," in *2022 IEEE Energy Conversion Congress and Exposition (ECCE)*. IEEE, 2022, pp. 1–6. [Online]. Available: https://ieeexplore.ieee.org/document/9947751

[6] R. G. Coe, G. Bacelli, D. Patterson, and D. G. Wilson, "Advanced WEC Dynamics & Controls FY16 testing report," Sandia National Labs, Albuquerque, NM, Tech. Rep. SAND2016-10094, October 2016. [Online]. Available: https://doi.org/10.2172/1330189

[7] M. Ancellin and F. Dias, "Capytaine: a python-based linear potential flow solver," *Journal of Open Source Software*, vol. 4, no. 36, p. 1341, 2019. [Online]. Available: https://doi.org/10.21105/joss.01341

[8] J. Falnes, *Ocean Waves and Oscillating Systems: Linear Interactions Including Wave-Energy Extraction*. Cambridge University Press, 2002. [Online]. Available: https://doi.org/10.1017/CBO9780511754630

[9] R. Coe, G. Bacelli, S. Spencer, D. Forbush, and K. Dullea, "MASK3 for advanced WEC dynamics and controls," Marine and Hydrokinetic Data Repository (MHKDR); Sandia National Laboratories, Tech. Rep. SAND2019-15428, 2019. [Online]. Available: https://dx.doi.org/10.15473/1581762

[10] D. C. Karnopp, D. L. Margolis, and R. C. Rosenberg, *System Dynamics: Modeling, Simulation, and Control of Mechatronic Systems, 5th Edition*. Wiley, 2012. [Online]. Available: https://books.google.com/books?id=8B5guy26PcQC

[11] G. Bacelli, "Optimal control of wave energy converters," PhD, National University of Ireland, Maynooth, Maynooth, Ireland, 2014. [Online]. Available: http://mural.maynoothuniversity.ie/6753/

[12] G. Bacelli and J. V. Ringwood, "Numerical optimal control of wave energy converters," *IEEE Transactions on Sustainable Energy*, vol. 6, no. 2, pp. 294–302, 2014. [Online]. Available: https://doi.org/10.1109/TSTE.2014.2371536

[13] G. Elnagar, M. Kazemi, and M. Razzaghi, "The pseudospectral Legendre method for discretizing optimal control problems," *IEEE Transactions on Automatic Control*, vol. 40, no. 10, pp. 1793–1796, 1995. [Online]. Available: https://doi.org/10.1109/9.467672

[14] R. G. Coe, S. Ahn, V. S. Neary, P. H. Kobos, and G. Bacelli, "Maybe less is more: considering capacity factor, saturation, variability, and filtering effects of wave energy devices," *Applied Energy*, vol. 291, p. 116763, 2021. [Online]. Available: https://doi.org/10.1016/j.apenergy.2021.116763

[15] E. Rusu and F. Onea, "A review of the technologies for wave energy extraction," *Clean Energy*, vol. 2, no. 1, pp. 10–19, 2018. [Online]. Available: https://doi.org/10.1093/ce/zky003